BASIC SCIENCES



m⁶A Modification of Profilin-1 in Vascular Smooth Muscle Cells Drives Phenotype Switching and Neointimal Hyperplasia via Activation of the p-ANXA2/STAT3 Pathway

Xiao-Fei Gao[®],* Ai-Qun Chen[®],* Hao-Yue Tang[®],* Xiang-Quan Kong[®],* Huan Zhang, Zhi-Mei Wang[®], Wei Lu[®], Li-Guo Wang, Feng Wang[®], Wen-Ying Zhou[®], Yue Gu[®], Guang-Feng Zuo[®], Zhen Ge, Jun-Jie Zhang[®], Shao-Liang Chen[®]

BACKGROUND: In-stent restenosis is characterized by a significant reduction in lumen diameter within the stented segment, primarily attributed to excessive proliferation of vascular smooth muscle cells (VSMCs) and neointimal hyperplasia. PFN1 (profilin-1), an actin-sequestering protein extensively studied in amyotrophic lateral sclerosis, remains less explored in neointimal hyperplasia.

METHODS: Utilizing single-cell RNA sequencing alongside data from in-stent restenosis patients and various experimental instent restenosis models (swine, rats, and mice), we investigated the role of PFN1 in promoting VSMC phenotype switching and neointimal hyperplasia.

RESULTS: Single-cell RNA sequencing of stenotic rat carotid arteries revealed a critical role for PFN1 in neointimal hyperplasia, a finding corroborated in stented swine coronary arteries, in-stent restenosis patients, PFN1sMC-IKO (SMC-specific PFN1 knockout) mice, and PFN1 overexpressed mice. PFN1 deletion was shown to suppress VSMC phenotype switching and neointimal hyperplasia in PFN1sMC-IKO mice subjected to a wire-injured model. To elucidate the observed discordance in PFN1 mRNA and protein levels, we identified that METTL3 (N6-methyladenosine methyltransferase) and YTHDF3 (YTH N6-methyladenosine RNA binding protein F3; N6-methyladenosine—specific reader) enhance PFN1 translation efficiency in an N6-methyladenosine—dependent manner, confirmed through experiments involving METTL3 knockout and YTHDF3 knockout mice. Furthermore, PFN1 was mechanistically found to interact with the phosphorylation of ANXA2 (annexin A2) by recruiting Src (SRC proto-oncogene, nonreceptor tyrosine kinase), promoting the phosphorylation of STAT3 (signal transducer and activator of transcription 3), a typical transcription factor known to induce VSMC phenotype switching.

CONCLUSIONS: This study unveils the significance of PFN1 N^6 -methyladenosine modification in VSMCs, demonstrating its role in promoting phenotype switching and neointimal hyperplasia through the activation of the p-ANXA2 (phospho-ANXA2)/ STAT3 pathway.

GRAPHIC ABSTRACT: A graphic abstract is available for this article.

Key Words: coronary artery disease ■ hyperplasia ■ muscle, smooth, vascular ■ percutaneous coronary intervention ■ profilins

Percutaneous coronary intervention with drug-eluting stent implantation stands as a primary treatment for obstructive coronary artery disease. Despite its efficacy, in-stent restenosis (ISR) remains a prevalent cause of stent failure, primarily attributed to the excessive proliferation of vascular smooth muscle cells

Correspondence to: Zhen Ge, MD, Department of Cardiology, Nanjing First Hospital, Nanjing Medical University, 68th Changle Rd, Nanjing 210006, China, Email gezhen666@163.com; Jun-Jie Zhang, MD, PhD, Department of Cardiology, Nanjing First Hospital, Nanjing Medical University, 68th Changle Rd, Nanjing 210006, China, Email jameszll@163.com; or Shao-Liang Chen, MD, PhD, Department of Cardiology, Nanjing First Hospital, Nanjing Medical University, 68th Changle Rd, Nanjing 210006, China, Email chmengx@126.com

*X.-F. Gao, A.-Q. Chen, H.-Y. Tang, and X.-Q. Kong contributed equally.

Supplemental Material is available at https://www.ahajournals.org/doi/suppl/10.1161/ATVBAHA.124.321399. For Sources of Funding and Disclosures, see page 2558.

© 2024 The Authors. Arteriosclerosis, Thrombosis, and Vascular Biology is published on behalf of the American Heart Association, Inc., by Wolters Kluwer Health, Inc. This is an open access article under the terms of the Creative Commons Attribution Non-Commercial-NoDerivs License, which permits use, distribution, and reproduction in any medium, provided that the original work is properly cited, the use is noncommercial, and no modifications or adaptations are made.

Arterioscler Thromb Vasc Biol is available at www.ahajournals.org/journal/atvb

p-ANXA2

Nonstandard Abbreviations and Acronyms

ANXA2 annexin A2

HRP horseradish peroxidase
ISR in-stent restenosis
m6A N6-methyladenosine

METTL3 N6-methyladenosine methyltransferase

PASMC primary mice aorta smooth

muscle cell

phospho-annexin A2

PDGF-BB platelet-derived growth

factor-BB

PFN1 profilin-1

PFN1SMC-IKO SMC-specific PFN1 knockout recombinant adeno-associated

virus

RIP RNA immunoprecipitation

Sc-RNA-seq single-cell RNA sequencing

VSMC vascular smooth muscle cell

(VSMCs) and neointimal hyperplasia.^{1,2} Our previous studies^{3,4} revealed that target lesion revascularization due to neointimal hyperplasia—induced myocardial ischemia occurred in over 5% of cases within 3 years after the index procedure. Employing single-cell RNA sequencing (Sc-RNA-seq) of stenotic rat carotid artery, we identified various cell types and their interrelations, in line with previous studies,^{5,6} emphasizing the pivotal role of VSMC phenotype switching in neointimal hyperplasia development.⁷

In this study, we utilized Sc-RNA-seq to investigate differentially expressed genes at the VSMC level between stenotic and normal carotid arteries.7 The candidate VSMC phenotype-related protein, PFN1 (profilin-1), a 14- to 17-kDa actin-sequestering protein extensively studied in amyotrophic lateral sclerosis but less explored in the cardiovascular field, 8,9 displayed increased protein expression in ISR patients and experimental ISR models. In addition, PFN1 exhibited a significant rise in N6-methyladenosine (m6A) levels, the most prevalent internal mRNA modification. PFN1 knockout demonstrated reduced VSMC proliferation, migration, and phenotypic switching in vitro, accompanied by a corresponding attenuation of neointimal hyperplasia in vivo. Furthermore, we uncovered that PFN1 binds to ANXA2 (annexin A2), increasing p-ANXA2 (phospho-ANXA2) expression and subsequently activating STAT3 (signal transducer and activator of transcription 3), thereby promoting VSMC phenotypic switching. These findings highlight, for the first time, the role of PFN1 m⁶A modification in VSMC, promoting phenotype switching and neointimal hyperplasia through the activation of the p-ANXA2/STAT3 pathway.

Highlights

- We have identified that PFN1 (profilin-1) knockout plays a crucial role in preventing neointimal hyperplasia by effectively inhibiting vascular smooth muscle cells' proliferation, migration, and phenotypic switching.
- The PFN1 N⁶-methyladenosine modification in vascular smooth muscle cells is a key contributor to the observed discordance between PFN1 mRNA and protein expression.
- Our findings indicate that PFN1 actively promotes vascular smooth muscle cell phenotype switching and neointimal hyperplasia by orchestrating the activation of the p-ANXA2 (phospho-annexin A2)/ STAT3 (signal transducer and activator of transcription 3) pathway.

METHODS

The data that support the findings of this study are available from the corresponding author upon reasonable request. Moreover, the Sc-RNA-seq data produced in the course of this study have been deposited into the Gene Expression Omnibus database under the accession number GSE174098.

Animals

The animal protocols and procedures were granted approval by the Animal Care and Use Committee of Nanjing First Hospital, Nanjing Medical University. Furthermore, all animals were housed in a temperature-controlled environment with a 12-hour light/dark cycle and provided with free access to fresh water and food. In this study, we used male rats to minimize potential interference from estrogen-related hormonal disturbances on the results.

In this study, we utilized genetically modified mice to investigate the roles of specific genes in our research. The floxed PFN1 mice (with LoxP [locus of X-over P1] sites flanking exon 2; CKOCMP-18643-PFN1-B6J-VA) and YTHDF3 (YTH N6-methyladenosine RNA binding protein F3)-global knockout mice (with LoxP sites flanking exon 3; KOCMP-229096-YTHDF3-B6N-VA) were obtained from Cyagen Biosciences. In addition, the floxed METTL3 (m6A methyltransferase) mice (with LoxP sites flanking exon 2-3; NM-CKO-190006, C57BL/6Smoc-METTL3^{(m1 (flox)Smoc)}) were sourced from Shanghai Model Organisms Center. MYH11-CreER^T2 (myosin, heavy polypeptide 11, smooth muscle-cyclization recombinase-estrogen receptor-Tamoxifen), TagIn (transgelin)-Cre (cyclization recombinase), and C57BL/6J mice were acquired from Cyagen Biosciences.

Rat Carotid Artery Balloon Injury

Male Sprague-Dawley rats weighing between 200 and 250 g were used for the carotid artery balloon-injury model. Briefly, a Fogarty balloon embolectomy catheter (12A0602F, Edwards Lifesciences) was introduced through the incision in the right external carotid artery. The balloon was inflated and withdrawn with rotation for 5 repetitions. After 4 weeks, the rats were humanely euthanized, and the carotid arteries were collected for further experimental analysis.

Murine Carotid Artery Wire Injury

Male 8-week-old mice were utilized for the carotid artery wire-injury model. Briefly, a guidewire (0.015-inch diameter; C-SF-15-15, Cook Medical LLC) was introduced through the incision in the right external carotid artery and pulled back to the carotid bifurcation in a rotating fashion for 5 repetitions. After 4 weeks, the mice were humanely euthanized, and the carotid arteries were collected for further experimental analysis.

Recombinant Adeno-Associated Virus Injection

A recombinant adeno-associated virus (rAAV) serotype 2/9 encoding Cre-inducible PFN1 (rAAV serotype 2/9-CMV [cytomegalovirus]-DIO [double-floxed inverse orientation]-PFN1-IRES [internal ribosome entry site]-mCherry-WPRE [woodchuck hepatitis virus posttranscriptional regulatory element]-hGh pA) and the control virus (rAAV serotype 2/9-CMV-DIO-mCherry-WPRE-hGh pA) were injected to TagIn-Cre mice via tail vein (5e¹¹ vg/mouse). The wire-injury operations for mice were performed 2 weeks after the rAAV injection. The rAAV packaging was performed by BrainVTA (Wuhan, China).

Swine-Stented Coronary Artery

Sections of swine-stented coronary arteries were generously provided by the laboratory of MicroPort Co. Ltd. (Shanghai, China). According to the laboratory's protocol, the left anterior descending artery of a swine underwent balloon injury initially, followed by the deployment of a drug-eluting stent (rapamycin-coated). Subsequently, after a 12-week period, coronary angiography was conducted to confirm the occurrence of significant ISR.

Cell Culture

Primary mouse VSMCs were isolated from the thoracic aortas of 10-week-old male mice (PASMCs [primary mice aorta smooth muscle cells]) by collagenase digestion. Isolated VSMCs were maintained in low-glucose DMEM (Dulbecco's modified eagle medium; Gibco BRL, Grand Island, NY) containing 10% fetal bovine serum (Gibco BRL, Grand Island, NY), and cells at passages 5 to 8 were used for further experiments.

Elastin Van Gieson Staining

Elastin Van Gieson staining was performed on 5-µm cryosections from murine carotid arteries. Cryosections were stained with Verhoeff Hematoxylin for 30 minutes, destained with 2% ferric chloride solution, and counterstained with Van Gieson solution (0.05% acid fuchsin in picric acid) for 65 s. Then, they were washed with ethanol, fully cleared with xylene, and sealed with neutral resin.

Immunohistochemical Staining

Sections were pretreated with heat-induced epitope retrieval in pH 6.0 10-mM sodium citrate buffer containing 0.05% tween-20 at 95 °C for 30 minutes. After quenching endogenous peroxidases with 3% $\rm H_2O_2$ and blocking with 4% goat serum phosphate-buffered saline (PBS), sections were incubated with primary antibodies (Major Resources Tables) overnight at 4 °C. Sections were incubated with biotinylated secondary antibodies and streptavidin conjugated to HRP (horseradish

peroxidase; BL050A, Biosharp). Finally, 3,3'-diaminobenzidine was used for chromogenic staining (BL732A, Biosharp).

Immunofluorescence Staining

Cryosections were fixed in 4% paraformaldehyde in PBS for 10 minutes and permeabilized with 0.1% Triton X-100 (in PBS). After blocking with 5% BSA for 1 hour, cryosections were incubated with primary antibodies (Major Resources Tables) overnight. Then, they were washed with PBS and labeled with FITC (fluorescein 5-isothiocyanate) or CY3 (sulfo-cyanine3) conjugated antibodies (Major Resources Tables). Finally, they were washed and sealed with 4′,6-diamidino-2-phenylindole Fluoromount-G (36308ES11, Yeasen). We used a Zeiss LSM-880 Meta laser confocal microscope with ×40 or ×63 oil to take pictures.

Migration Assay

Wound-healing and transwell migration assays were used to evaluate the migration of VSMCs. Cultured PASMCs were plated at 90% confluence in 6-well culture plates overnight. Subsequently, cells were manually wounded by scraping with a 200-µL pipette tip, followed by stimulation with PDGF-BB (platelet-derived growth factor-BB; 20 µg/L). Microscopic images were captured at 0 and 18 hours after the assay. For the transwell migration assays, $\approx 1\times10^4$ cells/well were seeded into a 24-well transwell plate (Corning). Following overnight incubation, cells were stimulated with PDGF-BB (20 µg/L). After 12 hours, cells on the upper surface were removed, and migrated cells on the lower surface were stained with 0.5% crystal violet for 10 minutes. Cell migration was observed under light microscopy.

Proliferation Assay

Cell Counting Kit-8 and 5-ethynyl-20-deoxyuridine assays were used to evaluate the proliferation of VSMCs. For the Cell Counting Kit-8 assay, ≈5×10³ cells/well were seeded into a 96-well plate overnight. Following stimulation with PDGF-BB (20 µg/L), Cell Counting Kit-8 solution (C0037, Beyotime) was added to each well and incubated for 2 hours at room temperature. Proliferation levels were assessed by measuring absorbance at 450 nm using a microplate reader. In the 5-ethynyl-20-deoxyuridine assay, around 2×104 cells/well were seeded into a 24-well plate overnight. After stimulation with PDGF-BB (20 µg/L), cell media was changed, and fresh media containing 10-µM 5-ethynyl-20-deoxyuridine (C0071S, Beyotime) was added. After a 2-hour incubation, cells were washed with PBS and fixed using 4% paraformaldehyde in PBS for 15 minutes. Hoechst stain was used to stain cell nuclei for 10 minutes. Image acquisition was automated using an Olympus microscope.

m⁶A mRNA Immunoprecipitation

A commercial riboMeRIP m⁶A Transcriptome Profiling Kit (C11051, Ribobio) was utilized following the manufacturer's instructions. In brief, total RNA was extracted using TRIzol and fragmented using RNA fragmentation buffer. Magnetic beads A/G were washed in immunocoprecipitation (IP) buffer and then incubated with the m⁶A-specific antibody (5 μ g/IP) for 30 minutes. The beads were washed with IP buffer, and 100-ng RNA was added to the beads along with RNase inhibitor

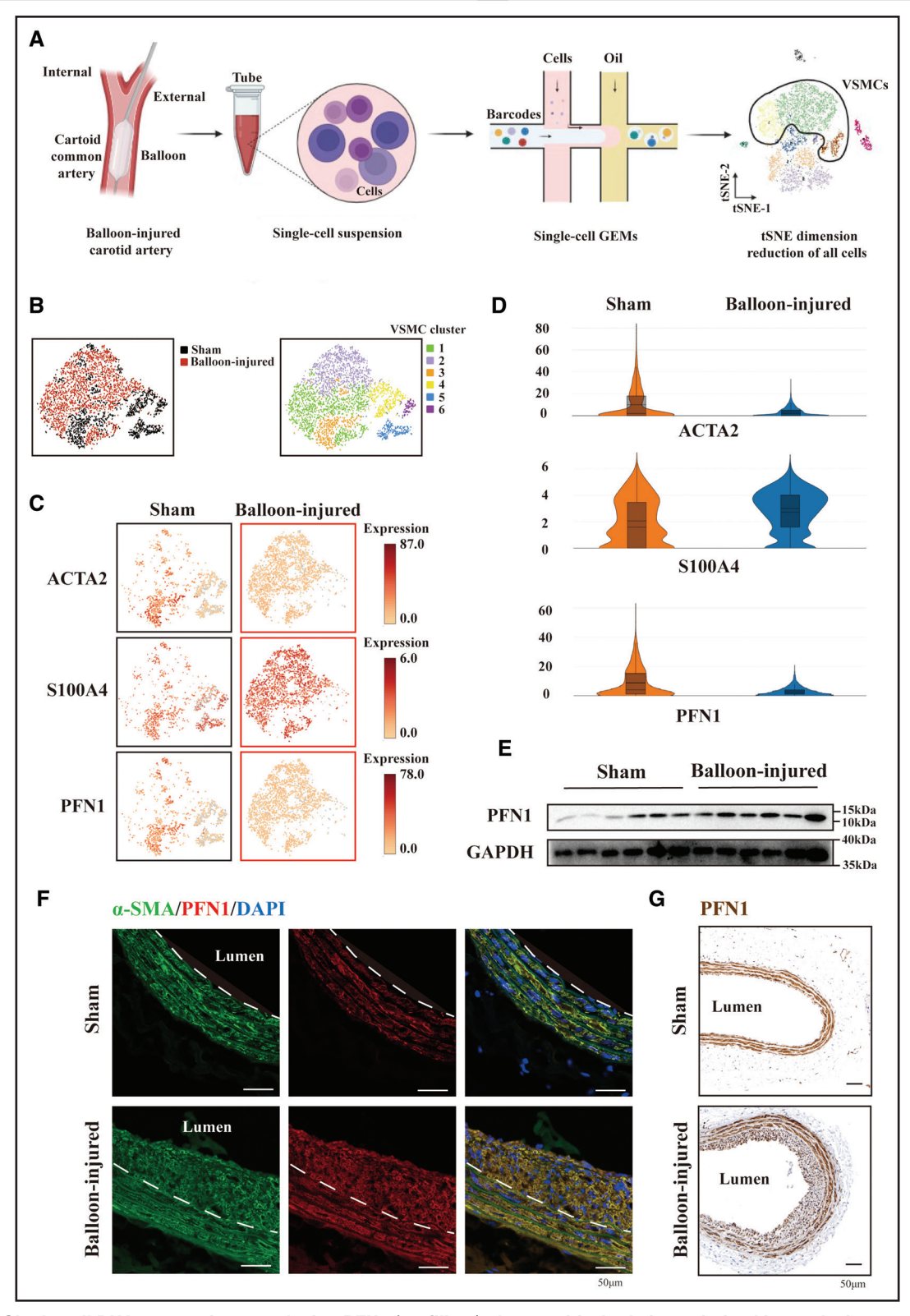


Figure 1. Single-cell RNA sequencing reveals that PFN1 (profilin-1) plays a critical role in neointimal hyperplasia.

A, Schematic diagram of balloon-injury procedure in rat right carotid arteries and flow chart of single-cell suspension. B, Distribution of balloon-injured and sham groups in vascular smooth muscle cells (VSMCs) and 6 clusters based on gene expression similarity. C, Expression and distribution of ACTA2, S100A4 (S100 calcium-binding protein A4), and PFN1 in each single cell of VSMCs. D, Violin plot visualizing the distribution of ACTA2, S100A4, and PFN1 mRNA expression and its probability density. E, Representative immunoblots and relative quantification analysis of PFN1 protein in rat carotid arteries (n=6 per group). F, Representative images showing double immunostaining for PFN1 (red) and α-SMA (actin alpha 2, smooth muscle, aorta; green) of rat carotid arteries in sham group and balloon-injured group (n=6 per group). G, Representative images showing immunohistochemistry for PFN1 of rat carotid arteries in sham group and balloon-injured group (n=6 per group). Scale bar, 50 μm. ACTA2 indicates actin alpha 2, smooth muscle, aorta; GEM, gel beads in emulsions; and tSNE, t-distributed stochastic neighbor embedding.

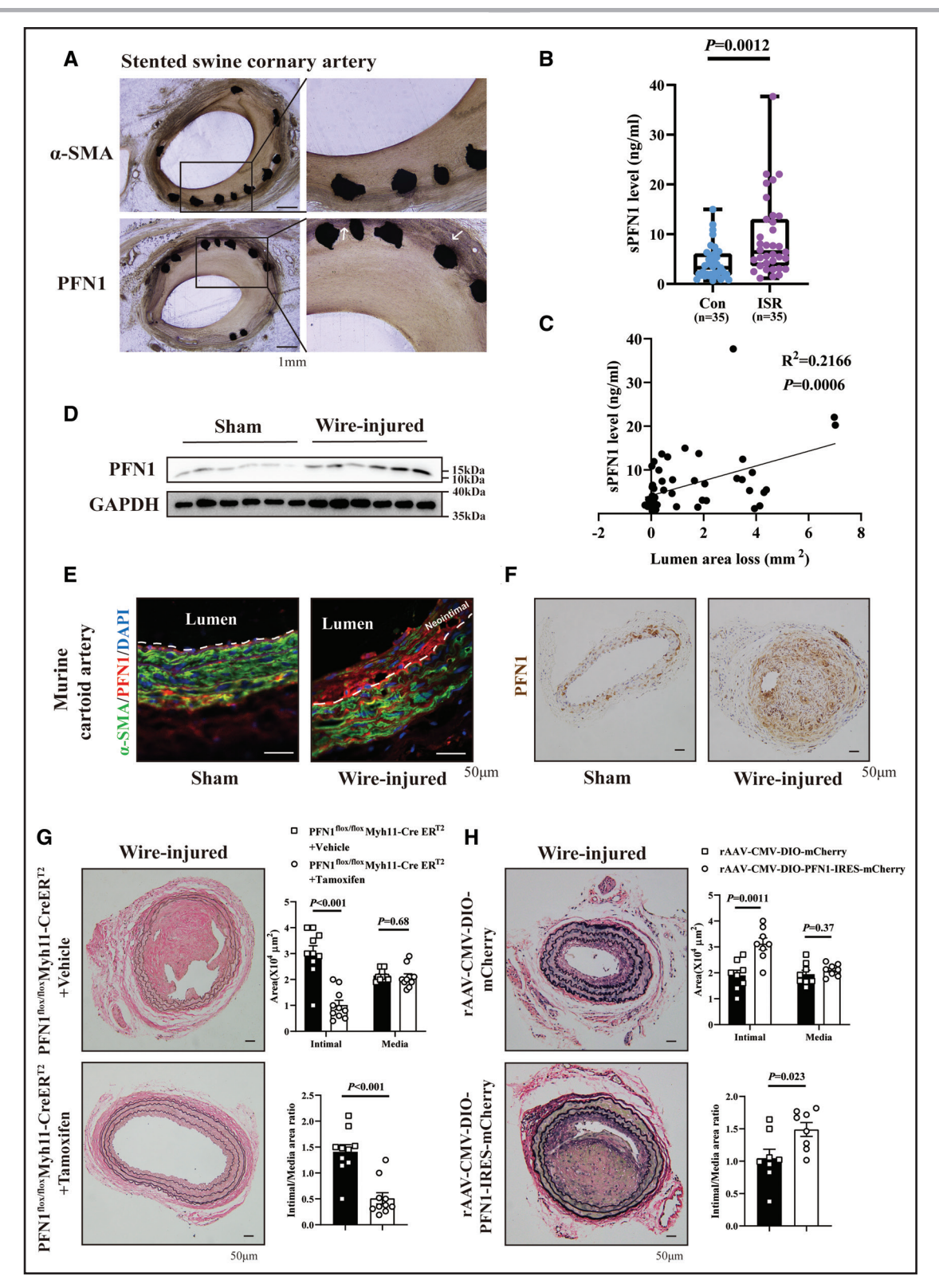


Figure 2. Multiple in vivo models confirm the participation of PFN1 (profilin-1) in neointimal hyperplasia.

A, Representative images showing immunohistochemistry for α-SMA (actin alpha 2, smooth muscle, aorta) and PFN1 in in-stent restenotic (ISR) area in swine (n=6). Scale bar, 1 mm. **B**, Serum quantification of PFN1 protein concentration from no-ISR patients (n=35) and ISR patients (n=35). Data are presented as box-and-whisker plots, with 75th and 25th percentiles; bars represent maximal and minimal values. Statistical comparison: unpaired *t* test. **C**, Correlation between serum PFN1 level and lumen area loss in 35 ISR patients; statistical comparison: Pearson correlation analysis. **D**, Representative immunoblots of PFN1 protein in murine carotid arteries in sham group and wire-injured group (n=6 per group). **E**, Representative images showing double immunostaining for PFN1 (red) and α-SMA (green) in uninjured and wire-injured murine carotid arteries (n=6 per group). Scale bar, 50 μm. **F**, Representative images showing immunohistochemistry for PFN1 in uninjured and (*Continued*)

and IP buffer. The mixture was tumbled at 4 °C for 2 hours. After washing with elution buffer (5× IP buffer, 20-mM m 6 A, RNase inhibitor, nuclease-free water), the m 6 A IP RNAs were recovered by ethanol precipitation. The final RNA sample was resuspended in 10 μ L of water.

RNA Immunoprecipitation

METTL3 and YTHDF3 RNA immunoprecipitation (RIP) was performed with a Magna RIPTM RNA-Binding Protein Immunoprecipitation Kit (17-700, Millipore) according to the manufacturers' instructions. Briefly, cell lysate was collected using RIP lysis buffer. Then, protein A/G magnetic beads were incubated with control IgG antibody (30000, Proteintech), METTL3 antibody (15073, Proteintech), or YTHDF3 antibody (25537, Proteintech) at room temperature for 30 minutes. Next, cell lysate was incubated with a bead-antibody mixture at 4 °C for 4 hours (10% as input). The samples were digested with proteinase K (HY-108717, MCE) to isolate the immunoprecipitation RNA and then analyzed by qPCR (quantitative PCR).

GST Pull-Down Assay

For analyzing of exogenous binding of PFN1 and ANXA2, cultured PASMCs were lysed in cell lysis buffer (P0013, Beyotime) containing 1× protease inhibitor (HY-K0010, MCE). The lysate was incubated with 10 μ g of purified GST (glutathione S-transferase) and GST-PFN1 protein. The GST protein was purified using IPTG (isopropyl-beta-D-thiogalactopyranoside; HY-15921, MCE), and the bound ANXA2 was detected through Western blot analysis.

Statistics

The results are expressed as mean \pm SEM. Statistical analyses, including unpaired t test, 1-way ANOVA, and Pearson correlation analysis, were used as appropriate. Differences with a significance level of P < 0.05 were considered statistically significant. Data were analyzed using SPSS (version 26.0) and GraphPad Prism, version 9.0.1 (GraphPad Software). For sc-RNA-seq data, detailed statistical analysis methods are outlined in the figure legends and our previous study.

RESULTS

sc-RNA-Seq Revealed That PFN1 Plays a Critical Role in Neointimal Hyperplasia

In our study, sc-RNA-seq sequencing was conducted using 10× Genomics technology in a rat carotid artery balloon-injury model to investigate the mechanisms underlying neointimal hyperplasia.⁷ Focusing on VSMCs,

we performed gene enrichment analysis, and visualized and classified these cells into 6 distinct clusters (Figure 1A and 1B). In addition, we displayed the top 200 differentially expressed genes (Table S1) in VSMCs between rat stenotic carotid artery and normal artery in Figure S1A. Notably, genes associated with VSMC phenotypic switching, including ACTA2 (actin alpha 2, smooth muscle, aorta; contractile phenotype) and S100A4 (S100 calcium-binding protein A4; synthetic phenotype), exhibited differential expression (Figure 1C and 1D). Of particular interest, the mRNA expression of PFN1 was found to decrease in the balloon-injured group, suggesting its involvement in VSMC phenotypic switching (Figure 1C and 1D; Figure S1B). However, Western blot analysis revealed an elevated protein level of PFN1 in balloon-injured carotid arteries compared with the sham group (Figure 1E; Figure S1C). Immunofluorescence and immunohistochemistry further confirmed PFN1's specific expression in VSMCs within rat carotid arteries, with higher expression in the balloon-injured group compared with sham group (Figure 1F and 1G). PFN1 was localized in VSMCs expressing α -SMA, reinforcing its association with neointimal hyperplasia progression (Figure 1F). In summary, our findings indicate differential expression of PFN1 between normal carotid arteries and vessels with neointimal hyperplasia.

Multiple In Vivo Model Confirmed the Participation of PFN1 in Neointimal Hyperplasia

Immunohistochemistry revealed significant expression of PFN1 in the vicinity of SMC-rich neointima and peri-strut areas of the swine coronary stent (Figure 2A). Serum samples from 35 patients with ISR and 35 patients without ISR, 1 year after coronary stent implantation, were collected (Table S2). Serum PFN1 expression was significantly higher in patients with ISR compared with those without ISR (9.181±1.330 versus 4.286±0.586 ng/mL; P=0.0012; Figure 2B). Importantly, the serum PFN1 level appeared to exhibit a linear trend with late lumen area loss, an indicator of the degree of restenosis (R2=0.2166; P=0.0006; Figure 2C). We also used a wireinjured mouse model, and Western blot analysis revealed a significant increase in PFN1 protein levels in wire-injured carotid arteries (Figure 2D; Figure S2A), while RT-qPCR (quantitative real-time PCR) found no significant difference in PFN1 mRNA levels between 2 groups (Figure S2B). Immunofluorescence and immunohistochemistry

Figure 2 Continued. wire-injured murine carotid arteries (n=6 per group). Scale bar, 50 μm. **G**, Representative images of elastin Van Gieson (EVG)—stained carotid artery sections from PFN1^{flox/flox} and PFN1^{SMC-IKO} (SMC-specific PFN1 knockout) mice underwent wire injury (n=10 per group). Scale bar, 50 μm. The right images show the quantification of intimal and medial area, and the ratio of intimal to medial area (n=10 per group). **H**, Representative images of EVG-stained carotid artery sections from PFN1^{WT} and PFN1^{SMC-OE} mice underwent wire injury (n=8 per group). Scale bar, 50 μm. The right images show the quantification of intimal and media area, and the ratio of intimal to media area (n=8 per group). All data are presented as mean±SEM; statistical comparison: unpaired *t* test. rAAV indicates recombinant adeno-associated virus serotype. CMV indicates cytomegalovirus; Con, control group; CreERT2, cyclization recombinase-estrogen receptor-Tamoxifen; DIO, double-floxed inverse orientation; GAPDH, glyceraldehyde-3-phosphate dehydrogenase; IRES, internal ribosome entry site; MYH11, myosin, heavy polypeptide 11, smooth muscle; and sPFN1, serum profilin-1.

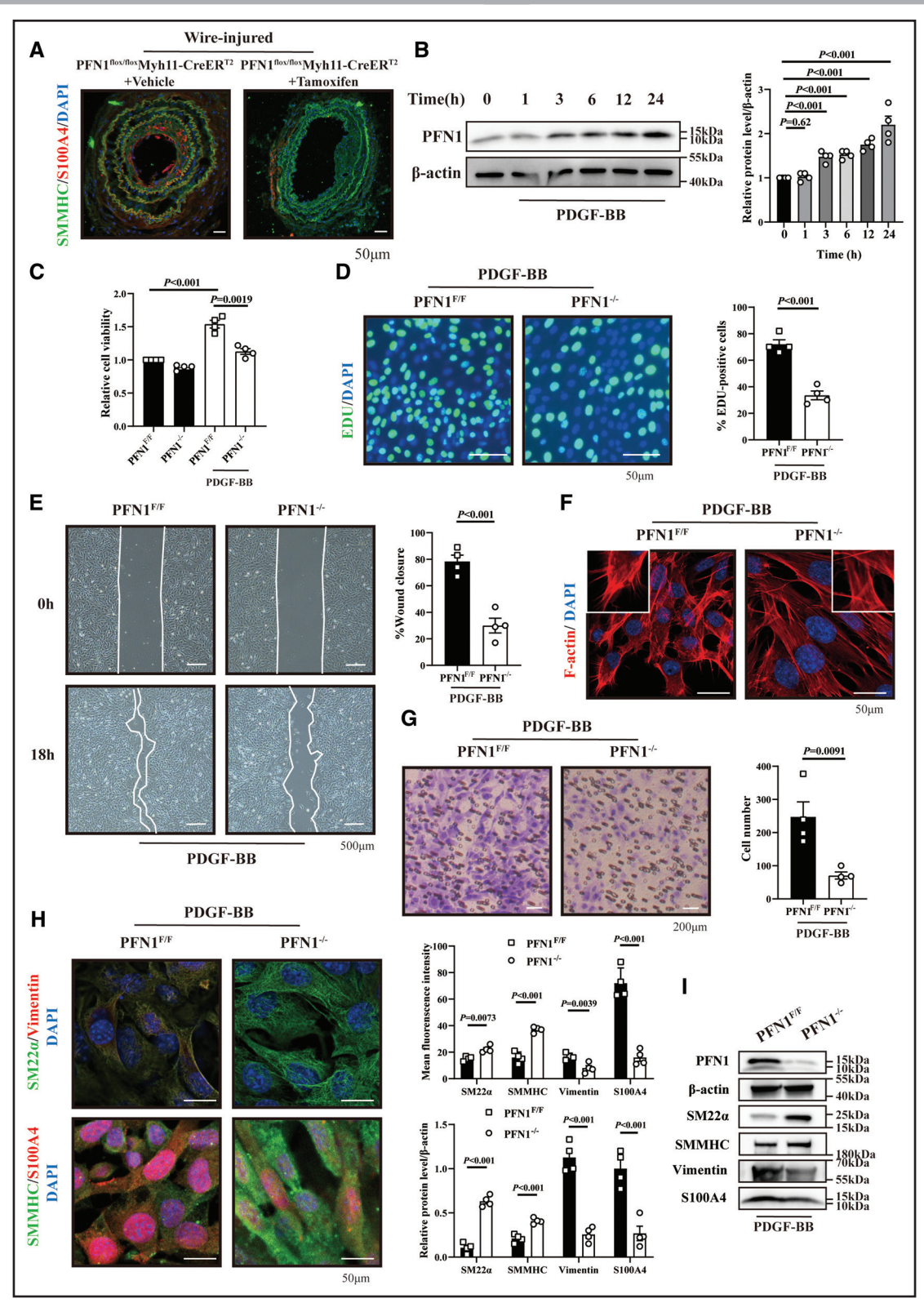


Figure 3. PFN1 (profilin-1) deletion suppresses vascular smooth muscle cell (VSMC) proliferation, migration, and phenotype switching.

A, Representative immunofluorescence staining showing the distribution of SMMHC (myosin, heavy polypeptide 11, smooth muscle) protein (green) and S100A4 (S100 calcium-binding protein A4) protein (red) in wire-injured carotid arteries from PFN1^{F/F} (PFN1^{flox/flox}) and PFN1^{-/-} (PFN1^{SMC-IKO} [SMC-specific PFN1 knockout]) mice (n=6 per group). B, Representative immunoblots and relative quantification analysis of PFN1 protein in primary mice aorta smooth muscle cells (PASMCs) stimulated with or without PDGF-BB (platelet-derived growth factor-BB; n=4). Statistical comparison: 1-way ANOVA with Tukey post hoc tests. C, Cell viability measured in PASMCs from PFN1^{F/F} and PFN1^{-/-} mice stimulated with PDGF-BB or not (n=4). Statistical comparison: 1-way ANOVA with Tukey post hoc tests. D, Representative immunofluorescence staining showing 5-ethynyl-20-deoxyuridine (EdU)-positive (Continued)

demonstrated that wire-injured carotid arteries expressed higher levels of PFN1 protein, particularly in the region of neointimal hyperplasia (Figure 2E and 2F), compared with the sham group.

Moreover, we generated PFN1^{SMC-IKO} (SMC-specific PFN1 knockout) and control mice (PFN1 flox/flox without tamoxifen induction; Figure S2C). Immunofluorescence of these mice after wire injury on carotid arteries demonstrated that PFN1 was localized in VSMCs expressing SMMHC (myosin, heavy polypeptide 11, smooth muscle), and PFN1 knockout in PFN1 SMC-IKO mice attenuated wire injury-induced neointimal hyperplasia compared with PFN1flox/flox mice (Figure S2D). Elastin Van Gieson staining supported that PFN1SMC-IKO mice exhibited a marked 50% decrease in intimal area and intimal/ medial ratio compared with PFN1 flox/flox mice (Figure 2G). Furthermore, elastin Van Gieson staining revealed that PFN1^{SMC-OE} mice with SMC-specific overexpression of PFN1 (Figure S3A and S3B) exhibited a significant promotion of neointimal hyperplasia compared with PFN1WT mice after wire injury on carotid arteries (Figure 2H). Neither knockout nor overexpression of PFN1 changed the baseline phenotype of VSMCs without injury in vivo (Figure S3C and S3D). Thus, our findings confirm the participation of PFN1 in neointimal hyperplasia via various in vivo models.

PFN1 Deletion Suppresses VSMC Proliferation, Migration, and Phenotype Switching

As previously reported, VSMC phenotype switching is a key mechanism in neointimal hyperplasia.^{5–7,10–12} Compared with wire-injured PFN1^{flox/flox} mice, immunofluorescence staining showed an increase in SMMHC and a decrease in S100A4 (Figure 3A) in PFN1^{SMC-IKO} mice. PDGF-BB has been proposed to be an important stimulus to promote VSMC differentiation.^{13,14} In vitro, PASMC were stimulated with PDGF-BB, resulting in an increase in PFN1 protein expression over the culture period (Figure 3B).

Subsequently, we isolated primary VSMCs from the aorta arteries of PFN1 SMC-IKO and PFN1 flox/flox mice. CCK8 kit assay indicated that PFN1 deletion impaired PDGF-BB-induced proliferation (Figure 3C), and 5-ethynyl-20-deoxyuridine incorporation assays demonstrated

that PFN1 deletion delayed proliferation in PDGF-BB-stimulated PASMCs (Figure 3D). Moreover, PDGF-BB-stimulated PASMCs from PFN1^{SMC-IKO} mice exhibited less migration than PFN1^{flox/flox} mice (Figure 3E). The migration capability was further assessed by F-actin distribution, revealing numerous filopodia in the gap regions of PDGF-BB-stimulated PASMCs from PFN1^{flox/flox} mice, while filopodia were scarce in PFN1^{SMC-IKO} mice (Figure 3F). PFN1 deletion also reduced the invasiveness of VSMCs, as validated by transwell chamber assay (Figure 3G).

Immunofluorescence staining illustrated differential expression of VSMC contractile markers (including SM22 α [transgelin2] and SMMHC) and synthetic markers (including vimentin and S100A4) after PDGF-BB stimulation, and PFN1 deletion reversed the PDGF-BB-induced VSMC phenotype switching from contractile to synthetic (Figure 3H and 3I). Thus, the current data demonstrate that PFN1 deletion suppresses VSMC proliferation, migration, and phenotype switching in both in vivo and in vitro models.

m⁶A Methylation Regulates the Translation Efficiency of PFN1 mRNA

In contrast to the protein level (depicted in Figure 3B), the mRNA level of PFN1 remained unaltered following PDGF-BB treatment (Figure 4A), hinting at potential posttranscriptional modifications. Although the protein level of PFN1 decreased over time after the protein translation inhibitor cycloheximide stimulation, no difference emerged between the control and PDGF-BBtreated groups (Figure 4B). Subsequently, actinomycin-D was used to evaluate RNA degradation efficiency, revealing no discernible difference between the control and PDGF-BB-treated groups (Figure 4C). In addition, stability analysis using doxorubicin for both DNA and RNA demonstrated no significant difference between the 2 groups (Figure 4D). Furthermore, ribosome profiling of different RNA fractions from PDGF-BB-treated PASMCs indicated that PFN1 mRNA was enriched in translation-active polysomes compared with the control group (Figure 4E).

Both PDGF-BB-pretreated and PDGF-BB-untreated PASMCs were subsequently treated with rapamycin,

Figure 3 Continued. cells (green) and Hoechst (blue) in PASMCs from PFN1^{F/F} and PFN1^{-/-} mice stimulated with PDGF-BB or not (n=4). Statistical comparison: unpaired *t* test. **E**, Representative images showing wound-healing assay results in PASMCs from PFN1^{F/F} and PFN1^{-/-} mice stimulated with PDGF-BB (n=4). Statistical comparison: unpaired *t* test. **F**, Representative immunostaining images showing expression of F-actin (red) and 4′,6-diamidino-2-phenylindole (DAPI; blue) in PASMCs from PFN1^{F/F} and PFN1^{-/-} mice stimulated with PDGF-BB (n=4). **G**, Representative images showing transwell assay results in PASMCs from PFN1^{F/F} and PFN1^{-/-} mice stimulated with PDGF-BB (n=4). Statistical comparison: unpaired *t* test. **H**, Representative immunostaining images showing expression of contractile marker proteins (SM22α [transgelin2] and SMMHC; green) and synthetic marker proteins (vimentin and S100A4; red) in PASMCs from PFN1^{F/F} and PFN1^{-/-} mice stimulated with PDGF-BB (n=4). Statistical comparison: unpaired *t* test. **I**, Representative immunoblots and quantification analysis of SM22α, SMMHC, vimentin, and S100A4 in PASMCs from PFN1^{F/F} and PFN1^{-/-} mice stimulated with PDGF-BB (n=4). Statistical comparison: unpaired *t* test. Scale bar, 50 μm. All quantitative data are expressed as mean±SEM. CreERT2 indicates cyclization recombinase-estrogen receptor-Tamoxifen; Myh11, myosin, heavy polypeptide 11, smooth muscle; and SM22α, transgelin2.

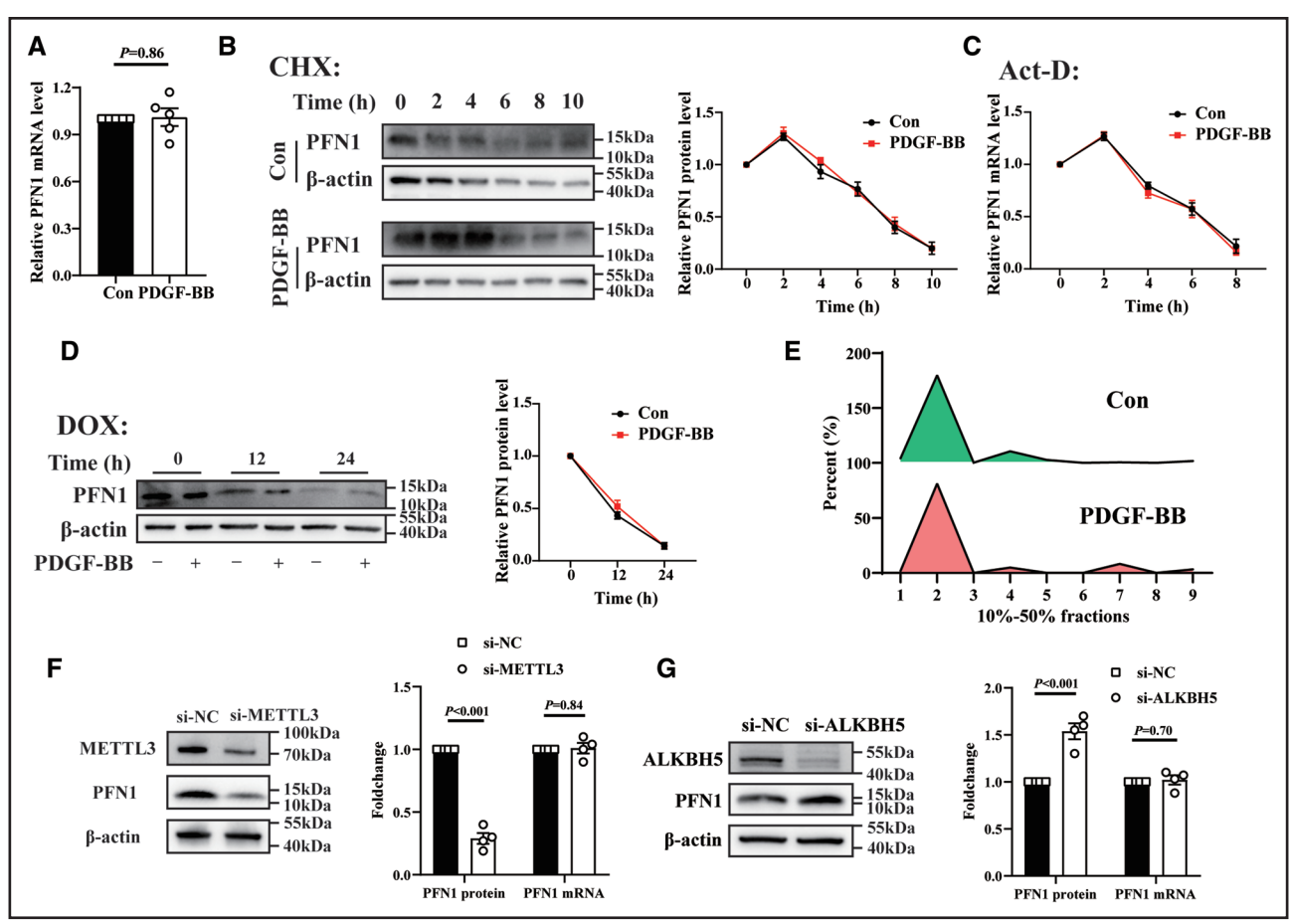


Figure 4. N⁶-methyladenosine (m⁶A) methylation regulates the translation efficiency of PFN1 (profilin-1) mRNA.

A, RT-qPCR (quantitative real-time PCR) assay assessing the mRNA level of PFN1 in primary mice aorta smooth muscle cells (PASMCs) stimulated with or without PDGF-BB (platelet-derived growth factor-BB; n=5). Statistical comparison: unpaired *t* test. B, Representative immunoblots and quantification analysis of PFN1 protein in cycloheximide (CHX)-treated PASMCs stimulated with PDGF-BB or not (n=4).

C, RT-qPCR assay assessing the mRNA level of PFN1 in actinomycin-D (Act-D)-treated PASMCs stimulated with PDGF-BB or not (n=4).

D, Representative immunoblots and quantification analysis of PFN1 protein in doxorubicin (DOX)-treated PASMCs stimulated with PDGF-BB or not (n=4).

E, Polysome profiling of PASMCs stimulated with PDGF-BB or not. PFN1 mRNA in different ribosome fractions was extracted and subjected to qPCR analysis. F, PASMCs were transected with si-NC or si-METTL3 (N⁶-methyladenosine methyltransferase), followed by stimulation with PDGF-BB or not. Representative immunoblots and quantification analysis of PFN1 protein and PFN1 mRNA (n=4).

Statistical comparison: unpaired *t* test. G, PASMCs were transected with si-NC or si-ALKBH5, followed by stimulation with PDGF-BB or not. Representative immunoblots and quantification analysis of PFN1 mRNA (n=4). Statistical comparison: unpaired *t* test. All quantitative data are expressed as mean±SEM. Con indicates control group.

an inhibitor of cap-dependent but not cap-independent translation. No obvious differences in PFN1 levels were observed between PDGF-BB-pretreated and PDGF-BB-untreated PASMCs (Figure S4). Thus, these data posited that m⁶A methylation, recognized as the most prevalent mRNA modification, ^{15–18} might regulate PFN1 translation efficiency. To validate this hypothesis, we individually silenced METTL3 (a key m⁶A methyltransferase) and ALKBH5 (a key m⁶A demethylase) in vitro to manipulate m⁶A methylation abundance. Our data indicated that silencing METTL3 led to a decrease in PFN1 protein levels (Figure 4F), whereas silencing ALKBH5 resulted in an increase in PFN1 protein levels (Figure 4G). These findings suggest a positive correlation between m⁶A methylation levels and PFN1 protein expression.

METTL3 Facilitates the Translation of m⁶A-Modified PFN1 mRNA

A dot-blot assay revealed an elevated overall expression level of transcripts with m⁶A methylation, particularly in PASMCs treated with PDGF-BB (Figure 5A). We also found that METTL3 exhibited the most prominent alteration in PASMC upon PDGF-BB stimulation (Figure S5A; Figure 5B). Moreover, immunohistochemistry assays illustrated increased METTL3 expression in neointimal hyperplasia arteries compared with normal arteries in both the rat balloon-injury model and the murine wireinjury model (Figure 5C). However, RT-qPCR data indicated that the knockdown of METTL3 did not affect the mRNA level of PFN1 (depicted in Figure 4F). In addition,

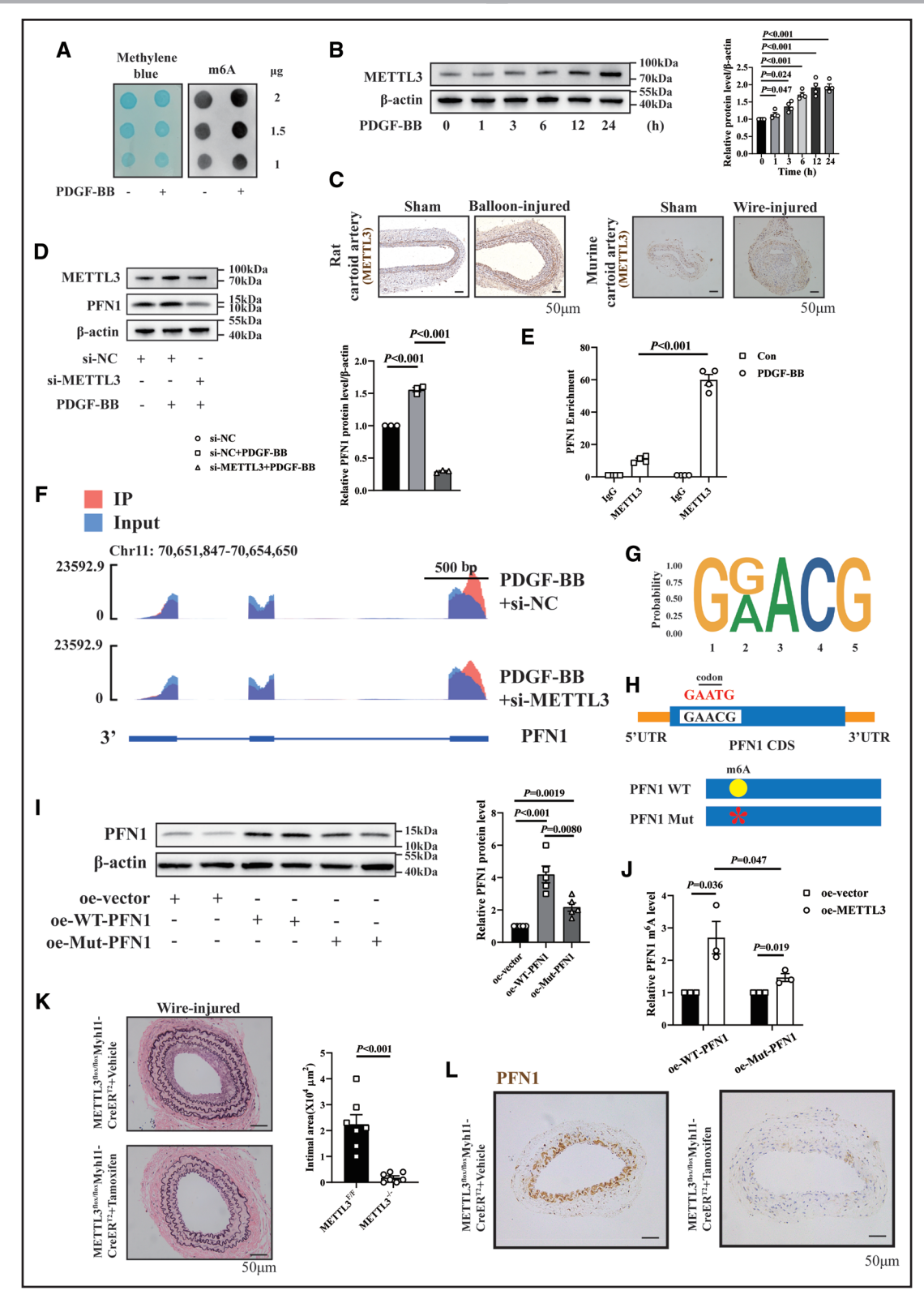


Figure 5. METTL3 (N⁶-methyladenosine methyltransferase) facilitates the translation of N⁶-methyladenosine (m⁶A)-modified PFN1 (profilin-1) mRNA.

A, RNA m⁶A dot-blot assays assessing m⁶A levels of total mRNA in primary mice aorta smooth muscle cells (PASMCs) stimulated with PDGF-BB (platelet-derived growth factor-BB) or not (n=3). **B**, Representative immunoblots and relative quantification analysis of METTL3 protein in PASMCs stimulated with or without PDGF-BB (n=4). Statistical comparison: 1-way ANOVA with Tukey post hoc tests. **C**, Representative immunohistochemistry of METTL3 in sham group, balloon-injured rat carotid arteries (**left**), and wire-injured murine carotid arteries (**right**; n=6). **D**, PASMCs were transfected with si-NC or si-METTL3, followed by stimulation with PDGF-BB or not. Representative immunoblots and quantification analysis of PFN1 protein (n=3). Statistical comparison: 1-way ANOVA with Tukey post hoc tests. **E**, RNA (*Continued*)

silencing METTL3 in PASMCs using si-RNA resulted in a decrease in PFN1 protein levels (Figure 5D).

To investigate the direct regulation of PFN1 expression by METTL3, we performed RIP and confirmed the binding between METTL3 protein and PFN1 mRNA, with PDGF-BB significantly enhancing their interaction (Figure 5E). Furthermore, m⁶A-RIP sequencing revealed m⁶A peaks in coding sequence regions, specifically from Chr11:70651847 to 70654650 (Figure 5F; Figure S5B and S5C), with the GGAC motif in the coding sequence identified by Hypergeometric Optimization of Motif EnRichment (Figure 5G). We also constructed a PFN1 plasmid to disrupt the GGAC motif with a synonymous mutation and a normal PFN1 plasmid with the same vector (Figure 5H). Western blot analysis revealed higher PFN1 expression in PASMCs with the wild-type PFN1 plasmid transfection compared with mutant PFN1 plasmids (Figure 5I; Figure S6A). Evaluation of m⁶A modification in wild-type PFN1 and mutant PFN1 showed lower levels in mutant PFN1 than in wild-type PFN1 with exogenous overexpressing METTL3 (Figure 5J).

Collectively, these findings suggest that m⁶A modifications of PFN1 mRNA regulate the expression of PFN1 protein, with METTL3 playing a crucial role in this regulatory process. Subsequently, we investigated whether METTL3 regulates PFN1 in vivo by generating METTL3^{SMC-IKO} mice and conducting wire-injured surgery on carotid arteries (Figure S6B and S6C). Elastin Van Gieson staining of these mice with wire-injured model indicated that METTL3^{SMC-IKO} delayed neointimal hyperplasia compared with METTL3^{Flox/flox} (Figure 5K), and immunohistochemistry in carotid arteries of METTL3^{SMC-IKO} mice demonstrated lower expression of PFN1 (Figure 5L). Overall, these data indicate that METTL3 facilitates the translation of m⁶A-modified PFN1 mRNA.

YTHDF3 Promotes PFN1 Translation Efficiency in an m⁶A-Dependent Manner

To identify potential m⁶A-specific readers, we observed significant changes in YTHDF3 expression in PASMCs treated with PDGF-BB (Figure 6A). Consistent with this,

sc-RNA-seq data revealed elevated YTHDF3 mRNA levels in VSMCs from balloon-injured rat carotid arteries (Figure 6B; Figure S7A). Western blot assay demonstrated a more substantial reduction in PFN1 protein levels with si-YTHDF3 compared with si-YTHDF1 (Figure 6C). In addition, the immunohistochemistry assay revealed a higher level of YTHDF3 protein in the wire-injured murine carotid artery compared with the sham group (Figure 6D). To confirm the association between the higher expression of YTHDF3 and m⁶A methylation, RIP experiments using an m⁶A antibody as the recruiter showed enhanced binding between YTHDF3 and m⁶A-modified transcripts in PDGF-BB-treated PASMCs (Figure 6E).

Furthermore, reducing YTHDF3 expression in PASMCs resulted in a decrease in PFN1 protein without altering its mRNA level (Figure S7B). YTHDF3 RIP analysis also indicated a significantly higher PFN1 protein level in this YTHDF3 fragment in PDGF-BBtreated PASMCs (Figure 6F). Finally, different RNA fractions isolated from PASMCs by ribosome profiling demonstrated that silencing METTL3 or YTHDF3 significantly reduced translation-active polysomes induced by PDGF-BB (Figure 6G). In addition, we generated heterozygous or homozygous YTHDF3 knockout mice (YTHDF3+/- or YTHDF3-/-; Figure S7C; Figure S8) and found a remarkedly decreased expression of PFN1 in the carotid arteries from YTHDF3-/mice compared with YTHDF3+/- mice, as detected by immunohistochemistry (Figure 6H). In summary, these findings collectively suggest that YTHDF3 promotes PFN1 translation efficiency in an m⁶A-dependent manner.

PFN1 Activates ANXA2/STAT3 Signaling Pathway to Promote VSMC Phenotype Switching

To screen for target proteins interacting with PFN1, ANXA2 emerged as a prominent candidate in the qualitative results of CO-IP (co-immunoprecipitation) and liquid chromatography-tandem mass spectrometry

Figure 5 Continued. immunoprecipitation (RIP)-qPCR analysis of PFN1 enrichment in PASMCs using the antibody of METTL3 or IgG heavy chain simulated with PDGF-BB or not, respectively (n=4). Statistical comparison: 1-way ANOVA with Tukey post hoc tests. **F**, m⁶A peaks enriched in coding sequence region of PFN1 gene from m⁶A-RIP-seq data. m⁶A enrichment of PFN1 coding sequence region markedly decreased when silencing METTL3 in PASMCs pretreated with PDGF-BB (n=1). **G**, Consensus sequence motified with differentially enriched m⁶A sites determined by a Hypergeometric Optimization of Motif EnRichment software. **H**, Schematic representation of m⁶A motif position in PFN1 mRNA. Schematic representation of wide-type (WT) and mutated (Mut) PFN1 (GAACG to GAATG) to investigate m⁶A roles on PFN1 protein expression. **I**, Representative immunoblots and relative quantification analysis of PFN1 protein in PASMCs transfected with WT-PFN1 and Mut-PFN1 plasmids for 48 hours (n=4). Statistical comparison: 1-way ANOVA with Tukey post hoc tests. **J**, The m⁶A level of PFN1 was detected using m⁶A-RIP-qPCR in HEK293T cells with cotransfection of human plasmids (n=3). Statistical comparison: 1-way ANOVA with Tukey post hoc tests. **K**, Representative images of elastin Van Gieson (EVG)-stained carotid artery sections from wire-injured METTL3^{flox/flox} and METTL3^{flox/flox} mice (n=7). Scale bar, 50 μm. All quantitative data are expressed as mean±SEM. CreERT2 indicates CreERT2, cyclization recombinase-estrogen receptor-Tamoxifen; and Myh11, myosin, heavy polypeptide 11, smooth muscle.

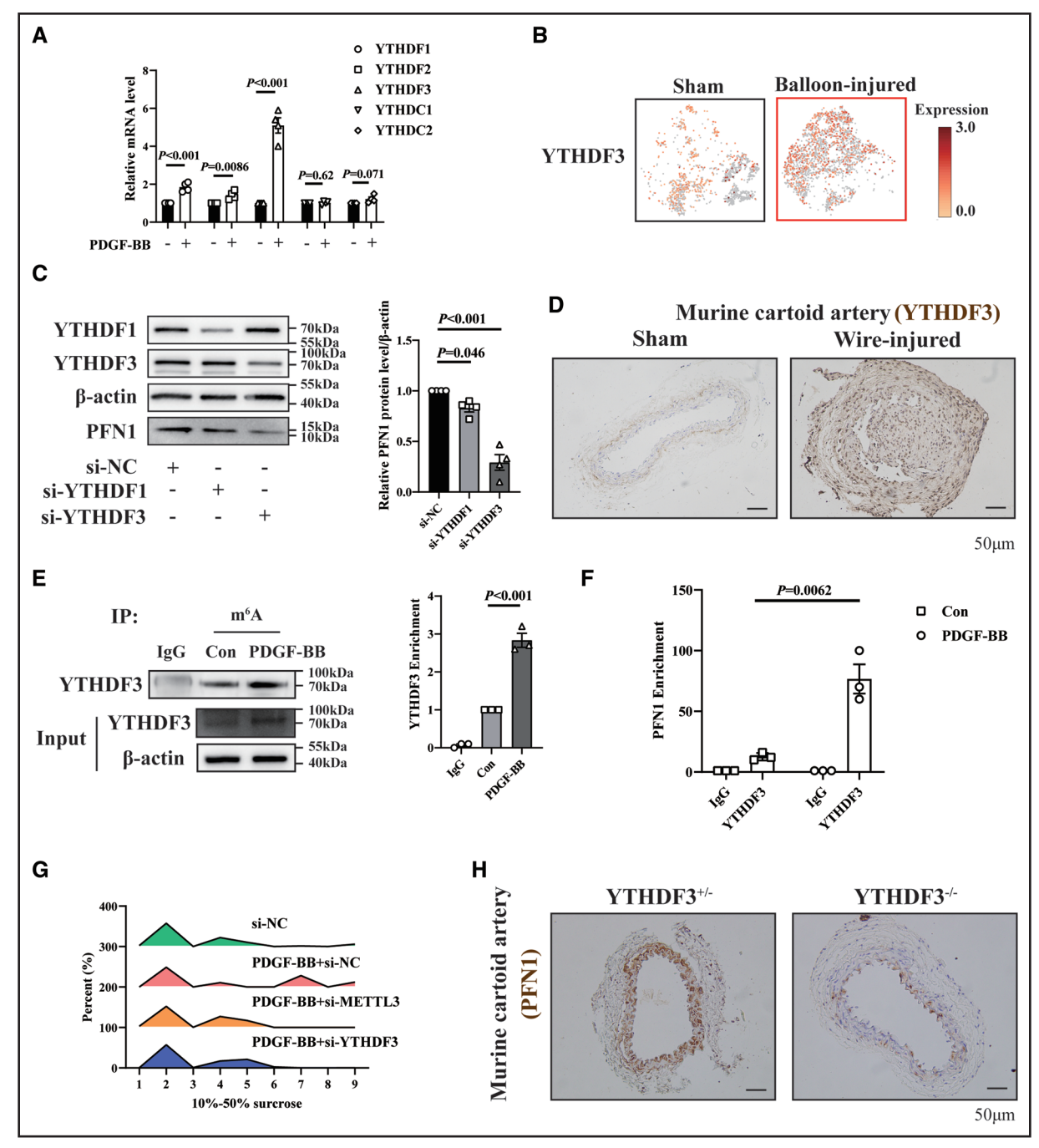


Figure 6. YTHDF3 (YTH N⁶-methyladenosine RNA binding protein F3) promotes PFN1 (profilin-1) translation efficiency in an N⁶-methyladenosine (m⁶A)-dependent manner.

A, RT-qPCR (quantitative real-time PCR) assay assessing mRNA expression in primary mice aorta smooth muscle cells (PASMCs) stimulated with PDGF-BB (platelet-derived growth factor-BB) or not (n=4). Statistical comparison: unpaired *t* test. **B**, Expression and distribution of YTHDF3 mRNA in every single cell of vascular smooth muscle cells (VSMCs) in single-cell RNA sequencing database. **C**, PASMCs were transfected with si-NC, si-YTHDF1, or si-YTHDF3. Representative immunoblots and quantification analysis of PFN1 protein (n=4). Statistical comparison: 1-way ANOVA with Tukey post hoc tests. **D**, Representative immunohistochemistry for YTHDF3 in uninjured and wire-injured murine carotid arteries (n=6). **E**, m⁶A-IP analysis of PASMCs stimulated with PDGF-BB or not for 24 hours using antibodies of m⁶A or IgG heavy chain, respectively (n=3). Statistical comparison: 1-way ANOVA with Tukey post hoc tests. **F**, RNA immunoprecipitation (RIP)-qPCR analysis of PASMCs stimulated with PDGF-BB or not for 24 hours using the antibody of YTHDF3 or IgG heavy chain (n=3). Statistical comparison: 1-way ANOVA with Tukey post hoc tests. **G**, Polysome profiling of PDGF-BB–pretreated/PDGF-BB–untreated PASMCs transfected with si-NC, si-METTL3 (m⁶A methyltransferase), and si-YTHDF3. PFN1 mRNA in different ribosome fractions was extracted and subjected to qPCR analysis. **H**, Representative images showing immunohistochemistry for PFN1 in carotid arteries from YTHDF3^{+/-} and YTHDF3^{-/-} mice (n=6). Scale bar, 50 μm. All quantitative data are expressed as mean±SEM. Con indicates control group; and IP, immunocoprecipitation.

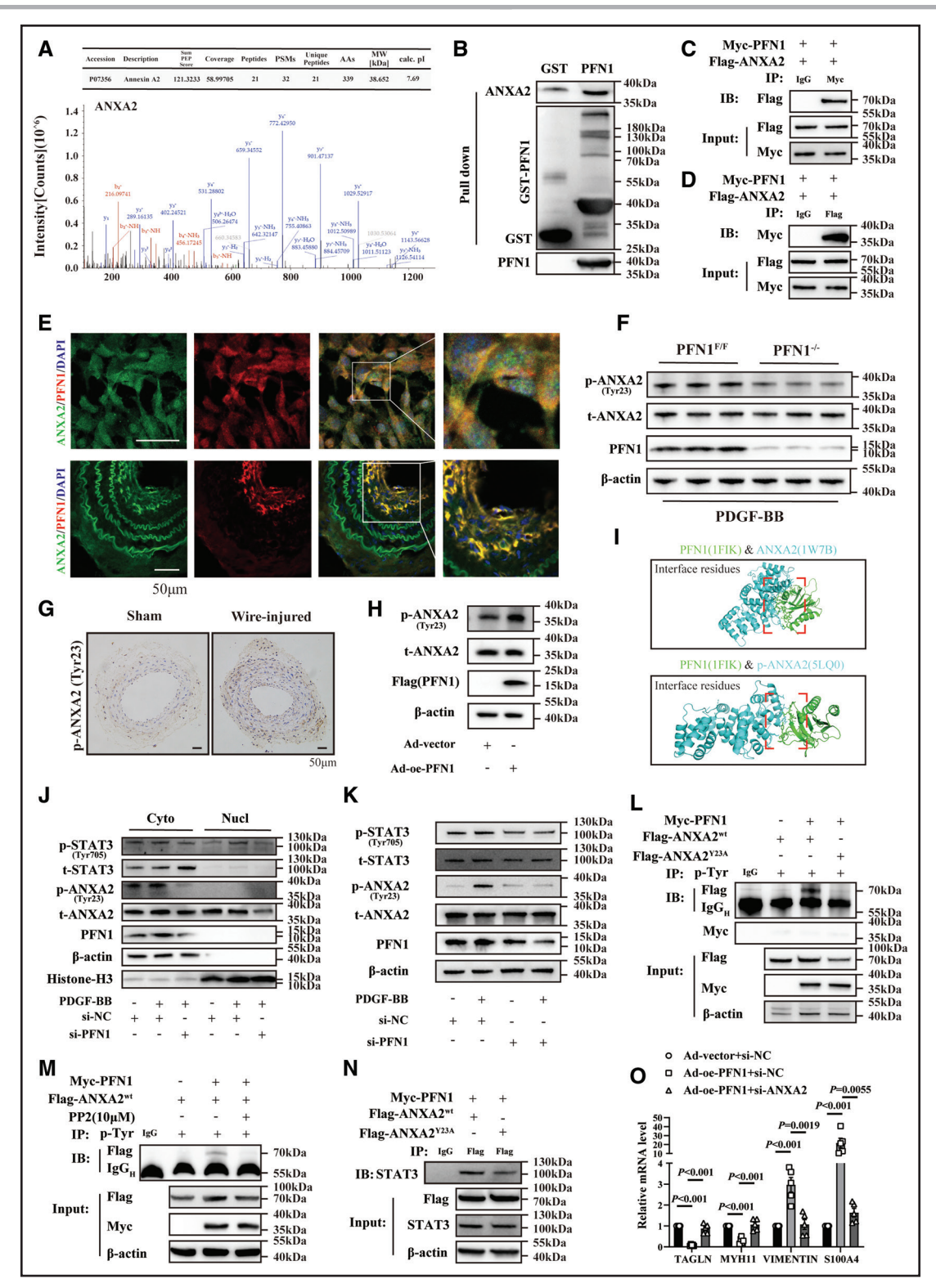


Figure 7. PFN1 (profilin-1) activates ANXA2 (annexin A2)/STAT3 (signal transducer and activator of transcription 3) signaling pathway to promote vascular smooth muscle cell (VSMC) phenotype switching.

A, Primary mice aorta smooth muscle cells (PASMCs) were stimulated with PDGF-BB (platelet-derived growth factor-BB) for 24 hours. The graph below shows the secondary mass spectrum of ANXA2 identified by mass spectrometry. **B**, Pull-down assays to pull down proteins interacting with PFN1. **C**, HEK293T cells were transfected with Myc-PFN1 and Flag-ANXA2 plasmids, and CO-IP (co-immunoprecipitation) analysis using Myc-PFN1 and IgG as the bait. **D**, HEK293T cells were transfected with Myc-PFN1 and Flag-ANXA2 plasmids, and CO-IP analysis using Flag-ANXA2 and IgG as the bait. **E**, Representative images showing double immunostaining for PFN1 (red) and ANXA2 (green) in PDGF-BB-treated PASMCs (n=3) and wire-injured murine carotid arteries (n=6). **F**, Representative immunoblots and relative quantification analysis of PFN1 and p-ANXA2 (phospho-ANXA2)/t-ANXA2 protein in PASMCs from PFN1^{F/F} and PFN1^{-/-} mice (n=4). Statistical comparison: (*Continued*)

in PASMCs treated with PDGF-BB (Table S3; Figure 7A). We utilized a GST pull-down assay confirming the interactions between PFN1 and ANXA2 (Figure 7B). CO-IP analysis also confirmed that PFN1 was coimmunoprecipitated with ANXA2 (Figure 7C and 7D). Immunofluorescence images demonstrated the colocalization of PFN1 and ANXA2, particularly in the neointima (Figure 7E). ANXA2 and its Tyr23 (tyrosine site 23)-phosphorylated form (Tyr23 p-ANXA2) have been implicated in cell transformation, metastasis, and angiogenesis. 19 In this study, first, Western blot analysis revealed significantly decreased expression of Tyr23 p-ANXA2 in PASMCs from PFN1 SMC-IKO mice compared with PFN1 flox/flox mice (Figure 7F; Figure S9A). Immunohistochemistry assay also showed a higher expression of Tyr23 p-ANXA2 in mice wire-injured carotid artery (Figure 7G). In addition, exogenous PFN1 overexpression promoted the phosphorylation of ANXA2 (Tyr23) in PASMCs (Figure 7H; Figure S9B). Prediction of the interaction probabilities through the GRAMM website suggested that PFN1 had a stronger binding affinity for ANXA2 than p-ANXA2 (Tyr23; Figure 7I).

Moreover, silencing PFN1 using si-RNA resulted in the reduction of phosphorylated ANXA2 in the cytoplasm of PASMCs (Figure 7J; Figure S9C). A typical signaling pathway ANXA2/STAT320,21 could be silenced upon PFN1 silencing (Figure 7J and 7K; Figure S9D). To identify whether PFN1 promotes the phosphorylation of ANXA2 (Tyr23) directly, we constructed an ANXA2 mutant plasmid (Y23A [replace site 23 tyrosine with alanine]) and performed CO-IP. Importantly, PFN1 significantly promoted the tyrosine phosphorylation of wildtype-ANXA2 but not Y23A-ANXA2 (Figure 7L). Thus, the PFN1 protein could not phosphorylate ANXA2 directly unless dependent on classical tyrosinase. Src (SRC proto-oncogene, nonreceptor tyrosine kinase) is well known to act as the main tyrosinase of ANXA2, and its phosphorylated form, pp60Src, promotes the

phosphorylation of ANXA2, especially at the Tyr23 site.^{22–24} We found a higher expression of Src in PASMCs treated with PDGF-BB, and PFN1 could not regulate Src directly (Figure S9E). More importantly, the tyrosine phosphorylation of wild-type-ANXA2 promoted by PFN1 could be inhibited by PP2 (an Src family kinase inhibitor; Figure 7M; Figure S9F). The CO-IP assay also confirmed that Tyr23 ANXA2 binds to STAT3 (Figure 7N). More importantly, overexpression of PFN1 in PASMCs promoted phenotype switching, and it could be reversed by transferring si-ANXA2 (Figure 7O). Together, these results suggest a novel molecular mechanism, whereby PFN1, through m⁶A modification in VSMC, promotes phenotype switching by activating the p-ANXA2/STAT3 pathway (Figure 8).

DISCUSSION

Despite decades of research on VSMC, our understanding of the mechanisms underlying VSMC phenotype switching remains incomplete, hindering effective prevention or treatment of neointimal hyperplasia. In this context, we propose several novel findings: (1) elevated levels of PFN1 protein are observed in patients with ISR and experimental ISR models involving swine, rats, and mice; (2) PFN1 m⁶A modification in VSMCs contributes to the discordant relationships between PFN1 mRNA and protein expression; (3) PFN1 knockout reduces the VSMC proliferation, migration, and phenotypic switching in vitro; in addition, it attenuates neointimal hyperplasia in vivo, underscoring the critical role of PFN1 in driving pathological changes associated with ISR; and (4) PFN1 promotes VSMC phenotype switching and neointimal hyperplasia by activating the p-ANXA2/STAT3 pathway. These findings collectively provide valuable insights that could pave the way for novel approaches in the prevention and therapeutic intervention of ISR, addressing a longstanding challenge in cardiovascular research.

Figure 7 Continued. unpaired t test. G, Immunohistochemistry for p-ANXA2 in uninjured and wire-injured murine carotid arteries (n=6). H, Representative immunoblots of PFN1 and p-ANXA2/t-ANXA2 protein in PASMCs transfected with Ad-vector or Ad-oe-PFN1 for 48 hours (n=4). I, The spatial conformation of PFN1 and t-ANXA2/p-ANXA2 and their interface residues visualized via the molecular visualization PyMOL software. J, Representative immunoblots of PFN1, p-ANXA2/t-ANXA2, and p-STAT3/t-STAT3 protein in separated cytoplasmic and nuclear proteins from PDGF-BB-untreated/PDGF-BB-pretreated PASMCs transfected with si-NC and si-PFN1 (n=4). Statistical comparison: 1-way ANOVA with Tukey post hoc tests. K, Representative immunoblots and relative quantification analysis of PFN1, p-ANXA2/t-ANXA2, and p-STAT3/t-STAT3 protein in PDGF-BB-untreated/PDGF-BB-pretreated PASMCs transfected with si-NC and si-PFN1 (n=4). Statistical comparison: 1-way ANOVA with Tukey post hoc tests. L, Myc-PFN1 plasmid with Flag-ANXA2 (wild-type) or Flag-ANXA2 (Y23A [replace site 23 tyrosine with alanine]) plasmid cotransfected into HEK293T cells, and CO-IP analysis using phosphorylated-Tyr antibody and IgG as the bait. M, Myc-PFN1 and Flag-ANXA2 (wild-type) plasmids cotransfected into HEK293T cells untreated or pretreated with PP2 (pp60Srcspecific inhibitor, 10 µM) for 24 hours. CO-IP analysis using phosphorylated-Tyr antibody and IgG as the bait. N, Myc-PFN1 plasmid with Flag-ANXA2 (wild-type) or Flag-ANXA2 (Y23A) plasmid cotransfected into HEK293T cells. Cell lysates immunoprecipitated with anti-Flag antibody and analyzed by immunoblotting with anti-STAT3 antibody. O, Ad-oe-PFN1, si-ANXA2, and their negative control cotransfected into PASMCs for 48 hours. RT-qPCR (quantitative real-time PCR) assay assessing mRNA expression of contractile markers (TAGLN [transgelin] and MYH11 [myosin, heavy polypeptide 11, smooth muscle]) and synthetic markers (vimentin and S100A4 [S100 calcium-binding protein A4]). Statistical comparison: 1-way ANOVA with Tukey post hoc tests. Scale bar, 50 µm. All quantitative data are expressed as mean±SEM. Flag indicates Flag-tag DYKDDDDK; Myc, Myc-tag EQKLISEEDL; oe, overexpression (plasmid); p-STAT3, phospho-signal transducer and activator of transcription 3 protein; t-ANXA2, total annexin A2 protein; Ad, adenovirus; t-STAT3, total signal transducer and activator of transcription 3 protein; and Tyr, tyrosine.

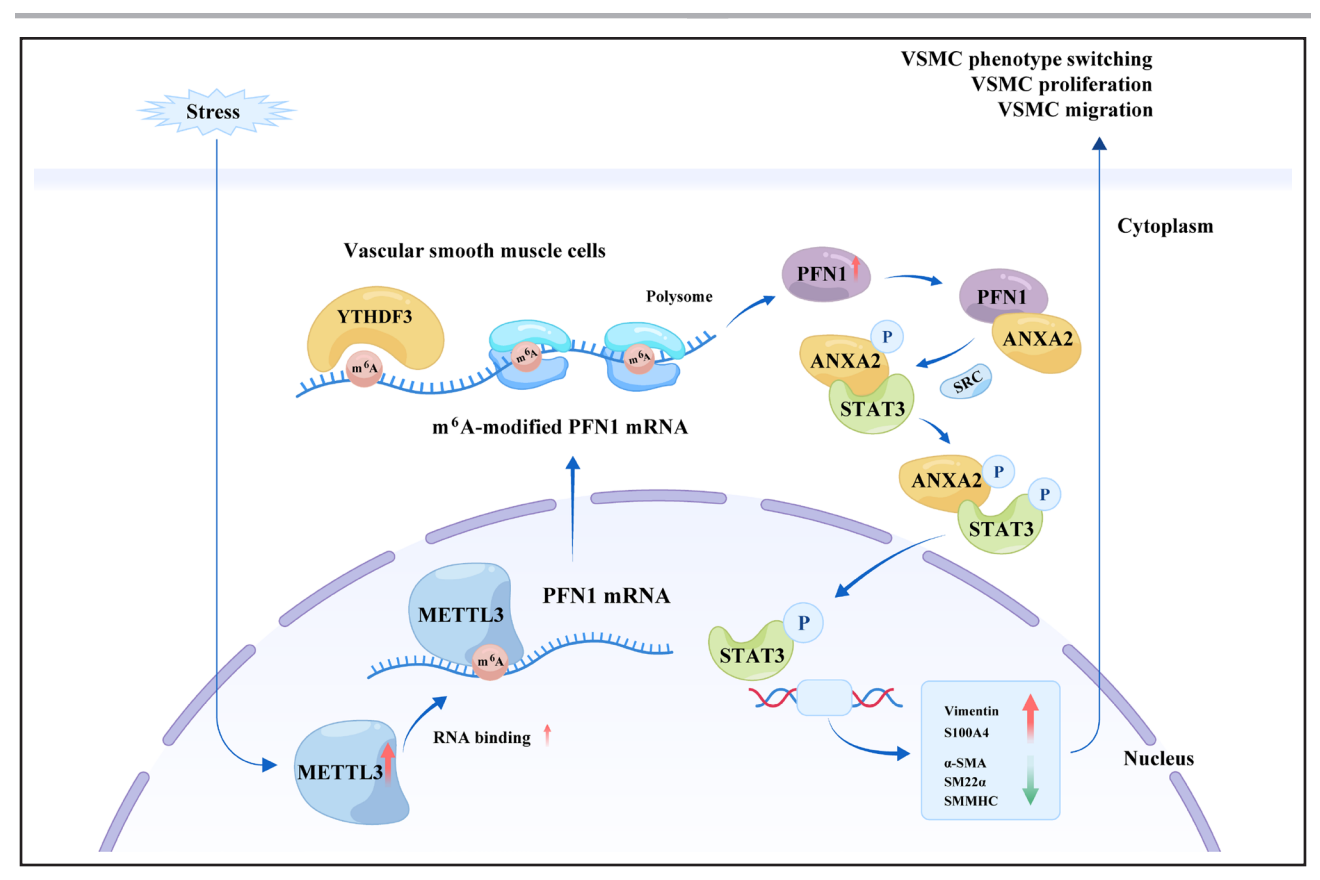


Figure 8. Proposed working model of PFN1 (profilin-1) in vascular smooth muscle cell (VSMC) in the context of atherosclerosis. Upon stimulation, VSMCs exhibit enhanced PFN1 translation efficiency via N⁶-methyladenosine (m⁶A) methyltransferase METTL3 (m⁶A methyltransferase) and the m⁶A-specific reader protein YTHDF3 (YTH N⁶-methyladenosine RNA binding protein F3) in an m⁶A-dependent manner. It has been mechanistically determined that the upregulation of PFN1 protein expression leads to the recruitment of Src (SRC proto-oncogene, nonreceptor tyrosine kinase), which, in turn, facilitates the phosphorylation of ANXA2 (annexin A2). This promotes the phosphorylation and nuclear translocation of STAT3 (signal transducer and activator of transcription 3), thereby inducing phenotypic switching in VSMCs. Src indicates SRC proto-oncogene, nonreceptor tyrosine kinase.

While PFN1 has been extensively studied in amyotrophic lateral sclerosis, its involvement in cardiovascular diseases has been limited by small sample sizes and less rigorous study designs. 8,9,25,26 In our study, we initially identified PFN1 at the VSMC level through Sc-RNA-seq data and subsequently validated it in patients with ISR and various experimental ISR models. Furthermore, our study confirmed that PFN1 knockout attenuated VSMC proliferation, migration, and phenotypic switching in vitro and reduced neointimal hyperplasia in vivo. These findings align with previous studies, suggesting that PFN1 may contribute to VSMC migration and hyperproliferation, potentially playing a role in chronic hypertension^{27,28} and asthma.^{29,30} In our study, we not only identified PFN1 at the VSMC level through Sc-RNA-seq but also validated its presence in multiple experimental models and clinical samples. Importantly, our study established a causal relationship between PFN1 and VSMC phenotypic switchinginduced neointimal hyperplasia, contributing to a deeper understanding of PFN1's role in vascular pathology.

A key discovery in our current study revolves around the distinct expression patterns of PFN1 mRNA and

protein, attributed to PFN1 m⁶A modification. Interestingly, the stability of PFN1 mRNA, transcription efficiency, and protein stability remained unchanged, while the translation efficiency of PFN1 exhibited a significant increase. Currently, m⁶A is recognized as the most prevalent posttranscriptional RNA modification, playing a role in various biological processes. 15-18,31 Given the involvement of m⁶A dynamics in PFN1 during neurogenesis³² and predictions from the SRAMP database, we hypothesized that PFN1 might undergo m⁶A methylation. Indeed, our validation data demonstrated that the protein expression of PFN1 was markedly inhibited in METTL3 or YTHDF3 knockout mice, indicating that the translation of PFN1 is regulated by METTL3 and YTHDF3 in an m⁶A-dependent manner. We also identified and validated the m⁶A methylation site of PFN1 with the GGAC motif in the coding sequence. While we have identified the sites involved, admittedly, the roles of other writers and readers in regulating the function of m⁶A RNA in neointimal hyperplasia have not been fully elucidated. Our next study will specifically focus on addressing this aspect.

An intriguing finding in this study is that the mRNA levels of PFN1 in rats decrease, while protein levels increase, yet no reduction in PFN1 mRNA levels was observed in mice. In fact, m⁶A methylation leads to an increase in protein levels by promoting mRNA translation, during which the absolute levels of mRNA may decrease, remain unchanged, or increase. 15-18,33 Therefore, the concentration of mRNA is not constant; the key to its role in increasing protein levels lies in promoting mRNA translation through the action of methyltransferases, demethylases, and m⁶A-binding proteins. Moreover, we confirmed an elevation of PFN1 protein levels through several ISR models, which are more crucial determinants of phenotypic outcomes. The observed decrease in PFN1 mRNA in rats and the unchanged levels in mice within this study might be attributed to species-specific and model variations, which warrant further investigation.

The identification of PFN1 as a key regulator in VSMC phenotype switching and neointimal hyperplasia also revealed its direct modulation of the p-ANXA2/STAT3 pathway. ANXA2, a Ca2+ phospholipid-binding protein, is well-established for its role in cell signaling transduction, influencing processes such as cell adhesion, migration, and proliferation.³⁴ The interaction between PFN1 and ANXA2, validated both in vivo and in vitro, highlights PFN1's role in influencing cellular processes related to cell adhesion, migration, and proliferation. In our study, the observed increase in Src and ANXA2 in VSMCs treated with PFN1 suggests a potential complex formation involving PFN1, Src, and ANXA2. Further experiments, notably with a Src inhibitor, demonstrated a significant attenuation in the phosphorylation of ANXA2 at the tyrosine 24 site. The involvement of Src kinaseinduced phosphorylation of ANXA2 further emphasizes the complexity of PFN1-mediated signaling.

CONCLUSIONS

Our study provided a significant advancement in understanding vascular biology by uncovering the pivotal role of PFN1 in VSMC phenotype switching and neointimal hyperplasia. The intricate interplay between PFN1, m⁶A modification, and the p-ANXA2/STAT3 pathway unravels novel molecular mechanisms underlying ISR.

ARTICLE INFORMATION

Received June 15, 2024; accepted October 16, 2024.

Affiliation

Department of Cardiology, Nanjing First Hospital, Nanjing Medical University, China.

Acknowledgments

S.-L. Chen, J.-J. Zhang, and Z. Ge designed and supervised the study. X.-F. Gao, A.-Q. Chen, H.-Y. Tang, and X.-Q. Kong performed the in vitro experiments and drafted the article. H. Zhang, Z.-M. Wang, W. Lu, F. Wang, and L.-G. Wang performed the in vivo experiments. W.-Y. Zhou, Y. Gu, and G.-F. Zuo performed the

adeno-associated virus administration and the informatics analysis. The authors thank Ms Ling Lin and Ms Hai-Mei Xu for their contributions to collecting the clinical data. The authors deeply appreciated Xuan Zhou, Xiao-Hua Yao, Yong-Bing Ba, and Jiao-Yang Dong at Shanghai OE Biotech Co. for their support of single-cell RNA sequencing and N⁶-methyladenosine-RNA immunoprecipitation sequencing.

Sources of Funding

The study was supported by the National Natural Science Foundation of China (NSFC; grants 81970307, 82100357, 82200385, and 82270344) and was jointly supported by the Jiangsu Natural Science Foundation (grant BK20221173), the Jiangsu Health Committee (grant H2019077), and the Nanjing Health Committee (grants JOX22007 and ZKX23030).

Disclosures

None.

Supplemental Material

Expanded Methods
Tables S1–S4
Figures S1–S9
Major Resources Tables

REFERENCES

- Alfonso F, Coughlan JJ, Giacoppo D, Kastrati A, Byrne RA. Management of in-stent restenosis. EuroIntervention. 2022;18:e103-e123. doi: 10.4244/EIJ-D-21-01034
- Giustino G, Colombo A, Camaj A, Yasumura K, Mehran R, Stone GW, Kini A, Sharma SK. Coronary in-stent restenosis: JACC state-of-the-art review. J Am Coll Cardiol. 2022;80:348–372. doi: 10.1016/j.jacc.2022.05.017
- Gao XF, Ge Z, Kong XQ, Kan J, Han L, Lu S, Tian NL, Lin S, Lu QH, Wang XY, et al; ULTIMATE Investigators. 3-year outcomes of the ULTIMATE trial comparing intravascular ultrasound versus angiography-guided drugeluting stent implantation. *JACC Cardiovasc Interv.* 2021;14:247–257. doi: 10.1016/j.jcin.2020.10.001
- Kan J, Zhang JJ, Sheiban I, Santoso T, Munawar M, Tresukosol D, Xu K, Stone GW, Chen SL, Investigators DI. 3-year outcomes after 2-stent with provisional stenting for complex bifurcation lesions defined by DEFI-NITION criteria. *JACC Cardiovasc Interv.* 2022;15:1310–1320. doi: 10.1016/j.jcin.2022.05.026
- Basatemur GL, Jorgensen HF, Clarke MCH, Bennett MR, Mallat Z. Vascular smooth muscle cells in atherosclerosis. *Nat Rev Cardiol*. 2019;16:727–744. doi: 10.1038/s41569-019-0227-9
- Miano JM, Fisher EA, Majesky MW. Fate and state of vascular smooth muscle cells in atherosclerosis. *Circulation*. 2021;143:2110–2116. doi: 10.1161/CIRCULATIONAHA.120.049922
- Gao XF, Chen AQ, Wang ZM, Wang F, Luo S, Chen SY, Gu Y, Kong XQ, Zuo GF, Chen Y, et al. Single-cell RNA sequencing of the rat carotid arteries uncovers potential cellular targets of neointimal hyperplasia. *Front Cardiovasc Med.* 2021;8:751525. doi: 10.3389/fcvm.2021.751525
- Allen A, Gau D, Roy P. The role of profilin-1 in cardiovascular diseases. J Cell Sci. 2021;134:jcs249060. doi: 10.1242/jcs.249060
- Paszek E, Zajdel W, Rajs T, Zmudka K, Legutko J, Kleczynski P. Profilin 1 and mitochondria-partners in the pathogenesis of coronary artery disease? Int J Mol Sci. 2021;22:1100. doi: 10.3390/ijms22031100
- Cao G, Xuan X, Hu J, Zhang R, Jin H, Dong H. How vascular smooth muscle cell phenotype switching contributes to vascular disease. *Cell Commun Sig*nal. 2022;20:180. doi: 10.1186/s12964-022-00993-2
- Chakraborty R, Chatterjee P, Dave JM, Ostriker AC, Greif DM, Rzucidlo EM, Martin KA. Targeting smooth muscle cell phenotypic switching in vascular disease. JVS Vasc Sci. 2021;2:79–94. doi: 10.1016/j.jvssci.2021.04.001
- Tang HY, Chen AQ, Zhang H, Gao XF, Kong XQ, Zhang JJ. Vascular smooth muscle cells phenotypic switching in cardiovascular diseases. *Cells*. 2022;11:4060. doi: 10.3390/cells11244060
- Jain M, Dhanesha N, Doddapattar P, Chorawala MR, Nayak MK, Cornelissen A, Guo L, Finn AV, Lentz SR, Chauhan AK. Smooth muscle cell-specific fibronectin-EDA mediates phenotypic switching and neointimal hyperplasia. J Clin Invest. 2020;130:295–314. doi: 10.1172/JCI124708
- Mao C, Ma Z, Jia Y, Li W, Xie N, Zhao G, Ma B, Yu F, Sun J, Zhou Y, et al. Nidogen-2 maintains the contractile phenotype of vascular smooth muscle cells and prevents neointima formation via bridging Jagged 1-Notch3 signaling. Circulation. 2021;144:1244–1261. doi: 10.1161/CIRCULATIONAHA.120.053361

- Boulias K, Greer EL. Biological roles of adenine methylation in RNA. Nat Rev Genet. 2023;24:143–160. doi: 10.1038/s41576-022-00534-0
- Deng X, Qing Y, Horne D, Huang H, Chen J. The roles and implications of RNA m⁶A modification in cancer. *Nat Rev Clin Oncol.* 2023;20:507–526. doi: 10.1038/s41571-023-00774-x
- Flamand MN, Tegowski M, Meyer KD. The proteins of mRNA modification: writers, readers, and erasers. *Annu Rev Biochem.* 2023;92:145–173. doi: 10.1146/annurev-biochem-052521-035330
- Sendinc E, Shi Y. RNA m6A methylation across the transcriptome. Mol Cell. 2023;83:428–441. doi: 10.1016/j.molcel.2023.01.006
- Grindheim AK, Hollas H, Raddum AM, Saraste J, Vedeler A. Reactive oxygen species exert opposite effects on Tyr23 phosphorylation of the nuclear and cortical pools of annexin A2. *J Cell Sci.* 2016;129:314–328. doi: 10.1242/jcs.173195
- Yin D, Hu ZQ, Luo CB, Wang XY, Xin HY, Sun RQ, Wang PC, Li J, Fan J, Zhou ZJ, et al. LINC01133 promotes hepatocellular carcinoma progression by sponging miR-199a-5p and activating annexin A2. Clin Transl Med. 2021;11:e409. doi: 10.1002/ctm2.409
- Pan H, Guo Z, Lv P, Hu K, Wu T, Lin Z, Xue Y, Zhang Y, Guo Z. Proline/ serine-rich coiled-coil protein 1 inhibits macrophage inflammation and delays atherosclerotic progression by binding to annexin A2. Clin Transl Med. 2023;13:e1220. doi: 10.1002/ctm2.1220
- Spijkers-Hagelstein JA, Mimoso Pinhancos S, Schneider P, Pieters R, Stam RW. Src kinase-induced phosphorylation of annexin A2 mediates glucocorticoid resistance in MLL-rearranged infant acute lymphoblastic leukemia. *Leukemia*. 2013;27:1063–1071. doi: 10.1038/leu.2012.372
- Fan Y, Si W, Ji W, Wang Z, Gao Z, Tian R, Song W, Zhang H, Niu R, Zhang F. Rack1 mediates tyrosine phosphorylation of Anxa2 by Src and promotes invasion and metastasis in drug-resistant breast cancer cells. *Breast Cancer Res.* 2019;21:66. doi: 10.1186/s13058-019-1147-7
- Zhao W, Zhang M, Wang G, Liu E, Jiang G, Zhang Y, Zhang D, Jian X, Zhao H, Zhang C, et al. GNAO T96S mutation abrogates the ability of wild-type GNAO to induce apoptosis by phosphorylating annexin A2 in natural killer/T cell lymphoma. *Cancer Sci.* 2022;113:2288–2296. doi: 10.1111/cas.15333

- Caglayan E, Romeo GR, Kappert K, Odenthal M, Sudkamp M, Body SC, Shernan SK, Hackbusch D, Vantler M, Kazlauskas A, et al. Profilin-1 is expressed in human atherosclerotic plaques and induces atherogenic effects on vascular smooth muscle cells. *PLoS One*. 2010;5:e13608. doi: 10.1371/journal.pone.0013608
- Paszek E, Zmudka K, Plens K, Legutko J, Rajs T, Zajdel W. Evaluation of profilin 1 as a biomarker in myocardial infarction. *Eur Rev Med Pharmacol Sci* 2020;24:8112–8116. doi: 10.26355/eurrev_202008_22497
- 27. Hassona MD, Abouelnaga ZA, Elnakish MT, Awad MM, Alhaj M, Goldschmidt-Clermont PJ, Hassanain H. Vascular hypertrophy-associated hypertension of profilin1 transgenic mouse model leads to functional remodeling of peripheral arteries. Am J Physiol Heart Circ Physiol. 2010;298:H2112–H2120. doi: 10.1152/ajpheart.00016.2010
- Chen JM, Guo RR, Gao Y, Wang CX, Yuan PN. Mechanism of action of Profilin-1 and fibulin-3 in vascular remodeling in hypertensive rats. Eur Rev Med Pharmacol Sci. 2019;23:8101–8108. doi: 10.26355/eurrev_201909_19028
- Tang DD. Critical role of actin-associated proteins in smooth muscle contraction, cell proliferation, airway hyperresponsiveness and airway remodeling. Respir Res. 2015;16:134. doi: 10.1186/s12931-015-0296-1
- Wang R, Liao G, Wang Y, Tang DD. Distinctive roles of Abi1 in regulating actin-associated proteins during human smooth muscle cell migration. Sci Rep. 2020;10:10667. doi: 10.1038/s41598-020-67781-1
- Sikorski V, Vento A, Kankuri E, Consortium IE. Emerging roles of the RNA modifications N6-methyladenosine and adenosine-to-inosine in cardiovascular diseases. Mol Ther Nucleic Acids. 2022;29:426–461. doi: 10.1016/j.omtn.2022.07.018
- Rockwell AL, Hongay CF. The m⁶A dynamics of profilin in neurogenesis. Front Genet. 2019;10:987. doi: 10.3389/fgene.2019.00987
- Liu Y, Yang D, Liu T, Chen J, Yu J, Yi P. N6-methyladenosine-mediated gene regulation and therapeutic implications. *Trends Mol Med.* 2023;29:454– 467. doi: 10.1016/j.molmed.2023.03.005
- Li YZ, Wang YY, Huang L, Zhao YY, Chen LH, Zhang C. Annexin A protein family in atherosclerosis. Clin Chim Acta. 2022;531:406–417. doi: 10.1016/j.cca.2022.05.009